SUPPLEMENTARY INFORMATION:

Supplementary Figures:

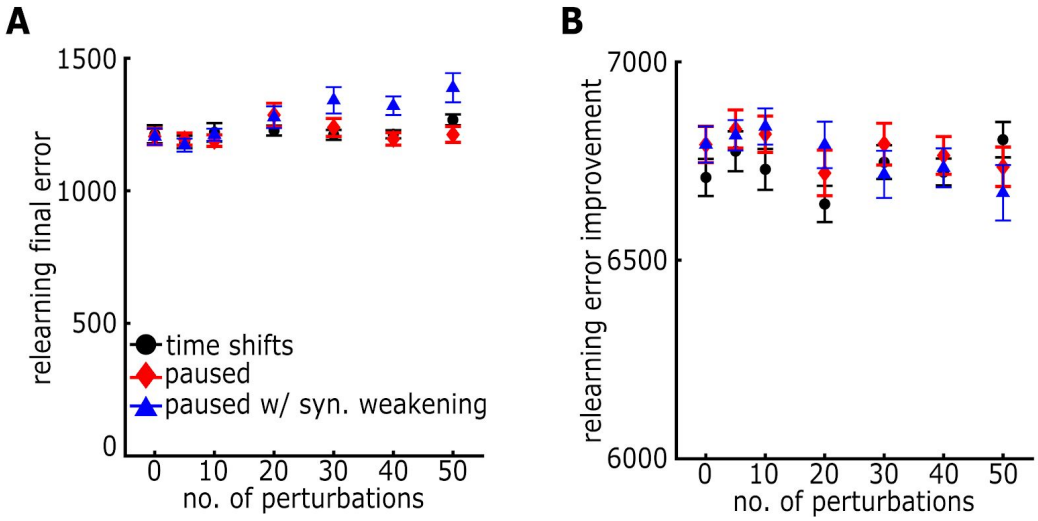

Figure S1. **A.** Comparison of final error after song re-learning. All perturbation schemes re-learn the shifted target song with equal accuracy across frequencies of perturbation except for the perturbation: 'paused with synaptic weakening,' which resulted in slightly less improvement in song at higher frequencies of HVC perturbations. Color schemes same as in Fig. 4. **B.** Comparison of error improvement after song re-learning. Error improvement is not significantly different across all perturbation schemes and frequency.

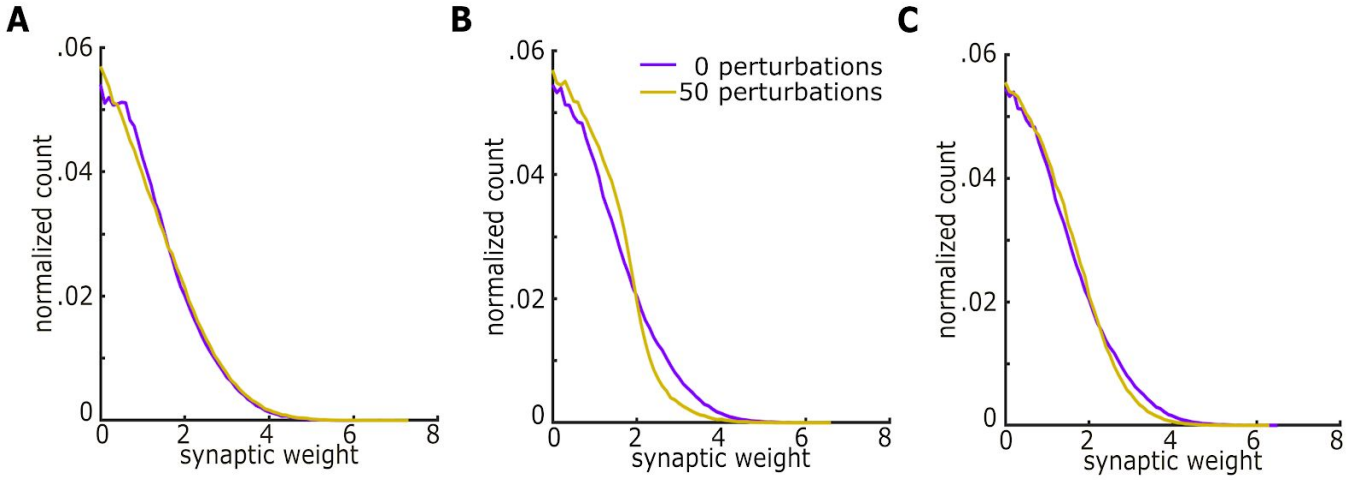

Figure S2. **A**. Distributions of synaptic weights after 10^5 maintenance trials for the paused perturbation scheme compared to the no perturbation control distribution. **B**. Distributions of synaptic weights after 10^5 maintenance trials for the paused with synaptic weakening perturbation scheme compared to the no perturbation, control distribution. **C**. Distributions of

synaptic weights after 10^5 maintenance trials for the time shifted perturbation scheme compared to the no perturbation, control distribution.

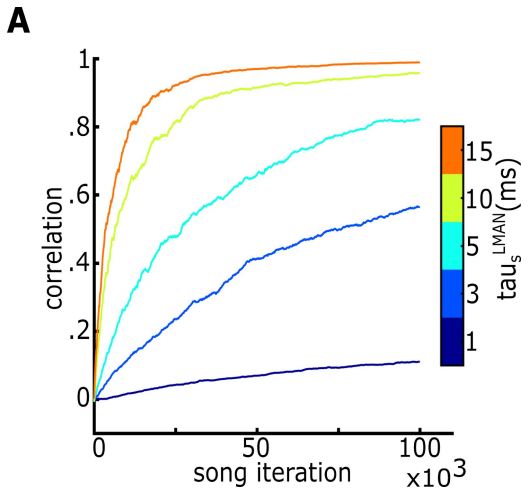

Figure S3. **A**. Example of the accumulation of average pairwise correlations over the course of 10^5 maintenance trials for varying time courses of LMAN inputs. As inputs from LMAN become more punctate in time, correlations across HVC projection strengths decrease. This shows that the build-up of correlations in the weight matrix is due to shared LMAN inputs. In the actual bird song system, LMAN synaptic inputs to RA are NMDA receptor mediated with long time courses (approximately 70-75 ms in adults) (1)

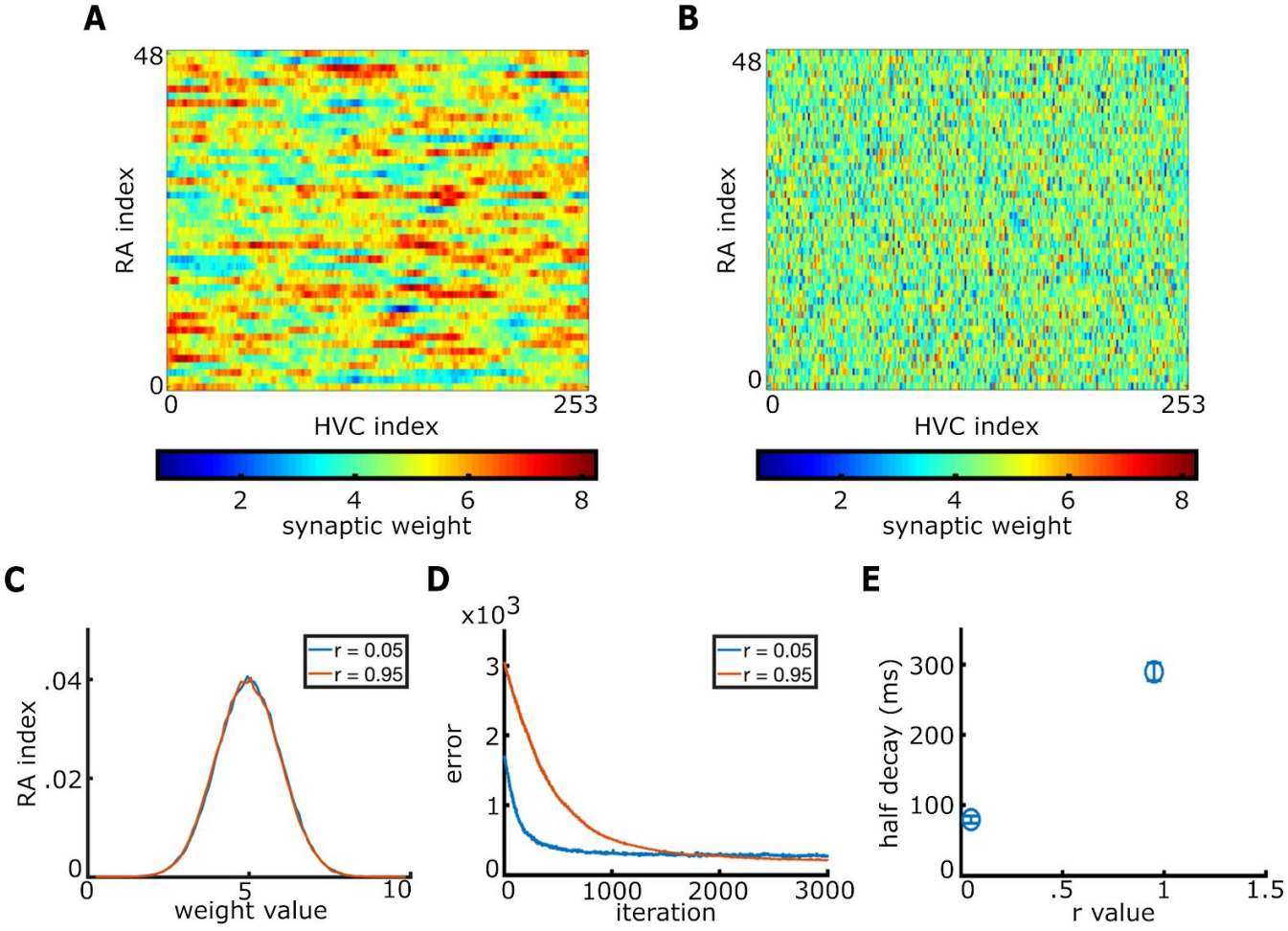

Figure S4. Learning speed depends on pairwise correlations of HVC synaptic weights in random Gaussian weight matrices. **A.** Example weight matrix with correlation between nearest neighbor HVC synaptic projection strengths, r = 0.95. **B.** Example weight matrix with correlation between nearest-neighbor, HVC synaptic projection strengths, r = 0.05. **C.** Comparison of synaptic weight distributions in weight matrices with r = 0.05 and r = 0.95. The overall distributions are identical and Gaussian distributed. Only the correlations between columns that differ. **D.** Average learning trajectory for each correlation level in the initial, random weight matrices before learning begins (over 25 trials per correlation level). **E.** Time to half decay of the traces in panel D. If the initial weight matrix has highly correlated columns, learning proceeds much more slowly.

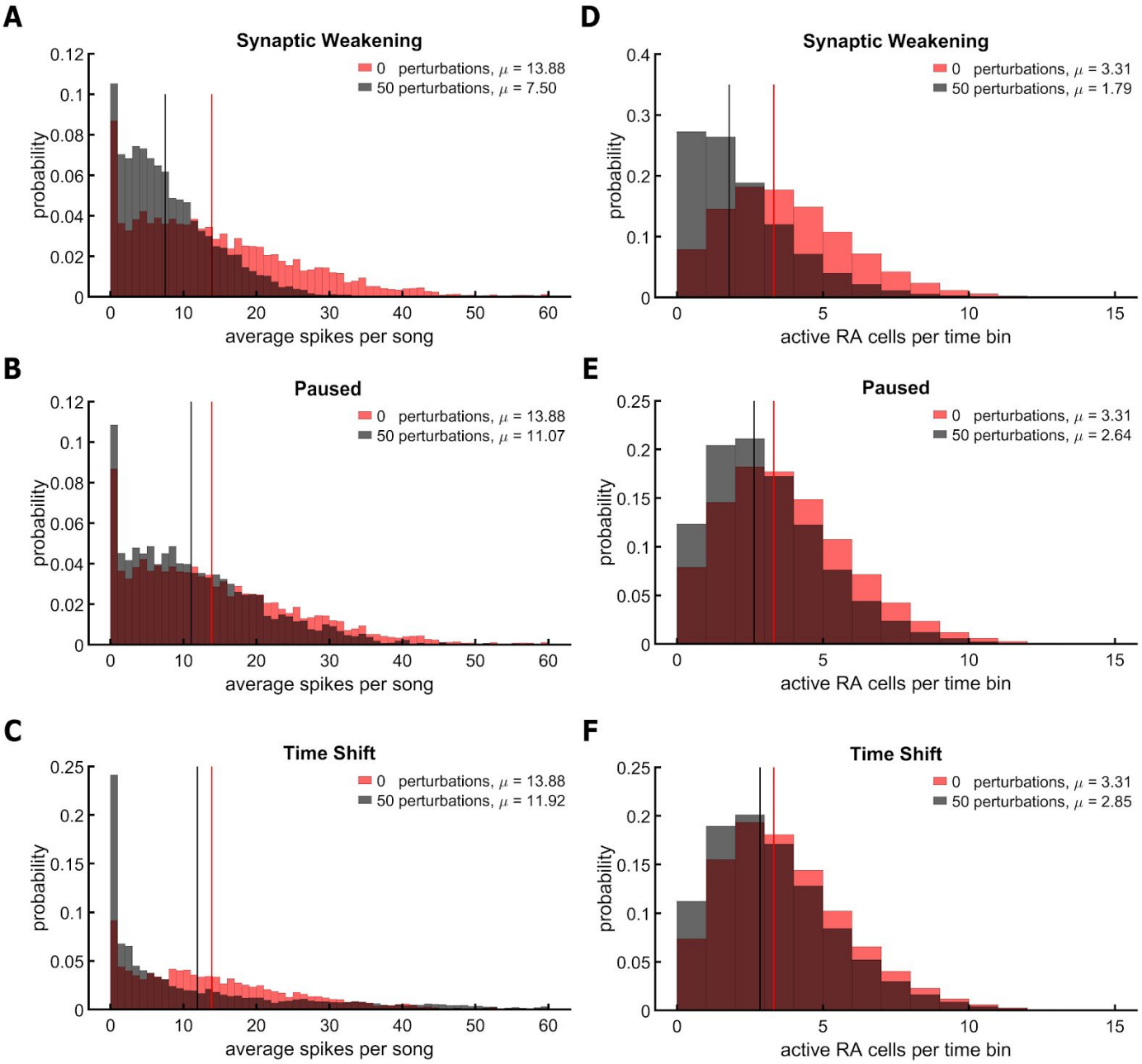

Figure S5: RA activity is more sparse when HVC is perturbed. **A.** Histogram of the average number of spikes in a song iteration for “paused with synaptic weakening.” Red and black vertical lines represent means of the distributions. **B.** Same as A but with “paused ” HVC perturbation scheme, and **C.** Same as A and B but “time shift " HVC perturbation. **D-F.** Histograms of the number of active cells per time bin of the song (time = 0.5 ms). Red and black vertical lines represent means of the distributions. D-F have the same HVC perturbation order as in A-C.

Statistical Significance:

To test whether the number of perturbations of each type affected the final error, the half time for relearning, the error from RA cell loss and the final weight correlations, we carried out one-way analysis of variance (ANOVA) using Prism (GraphPad Software). In all cases, there was a significant main effect of the number of perturbations ($p < 0.0001$ in each case).

Extended Methods:

In this section, we lay out the basic framework for the network and then describe the three different approaches utilized in the perturbations to HVC activity patterns. Following this, we give details on how we measured network robustness.

A. Base Model and Network Architecture

In this initial approach, the base model comprised three layers with feed-forward connectivity, representing the premotor network of HVC, RA and motor pools, with empiric synapses from LMAN driving variability (Fig. 1a,b).

1. Neuronal Parameters

Our base model is derived from that of Fiete et al., (2007)(2). We assume a model structure shown in Fig. 1b, with 500 active HVC neurons projecting to 48 RA neurons. Each RA neuron is represented as a single-compartment, conductance-based model. Each RA neuron projects to one of two motor pools, which are low-dimensional representations of song features, such as fundamental frequency or amplitude. The LMAN input to each RA neuron is taken to be an independent Poisson process.

Each neuron in the HVC and RA layers is modeled as a conductance-based leaky integrate-and-fire neuron:

$$C_m\,(dV_i/dt) = -g_L(V_i - V_L) - g_{E,i}(V_i - V_E) - g_{I,i}(V_i - V_I) \qquad (1)$$

where $g_{L,i}$, $g_{E,i}$, $g_{I,i}$ represent the leak, excitatory, and inhibitory conductance, respectively for the ith neuron. Within this model, a spike is generated when V_i crosses the threshold voltage V_θ, and is reset to V_{reset}.

a. HVC Layer

The onset times for HVC bursts were drawn from a uniform random distribution over the time-course of the motif. $g_{I,j}(t) = 0$ for all neurons. $g_{E,j}(t) = 0$ for all neurons at all times in the song motif, except for one 6-ms excitatory pulse with magnitude 0.13 mS/cm^2 to drive a single burst. The frequency and duration of the current pulses and subsequent bursts were chosen to mimic the actual song system (3).

b. RA Layer with LMAN Input

RA neurons receive excitatory input from HVC, and both excitatory and inhibitory input from LMAN. Biological LMAN neurons are glutamatergic and excitatory; we modeled this excitatory connection and also introduced an inhibitory component representing disynaptic inhibition from LMAN to RA via RA interneurons (4). This balanced synaptic input allows stable song over long time scales. In addition, there is weak, recurrent, inhibitory activity in RA.

In RA, the excitatory, synaptic conductances are described by:

$$g_{E,i}^{RA}(t) = 0.0024 \sum_j [W_{ij}\, s_j^{HVC}(t) + (s_i^{LMAN+}(t) + s_i^{LMAN-}(t))], \qquad (2)$$

where W_{ij} represents the synaptic weight from the jth HVC neuron to the ith RA neuron, s_j^{HVC} represents the synaptic activation level from the jth HVC neuron, and s_i^{LMAN+} represents the excitatory component of the synaptic activation from the LMAN input to the ith RA neuron, and s_i^{LMAN-} represents the inhibitory LMAN input. The recurrent inhibitory synaptic conductances in RA are described by:

$$g_{I,i}^{RA}(t) = (0.2/N_{RA}) \sum_i s_i^{RA}(t), \qquad (3)$$

where N_{RA} is the number of RA neurons. Following an action potential in neuron i, the synaptic activation $s_i(t)$ is increased by one, and decays exponentially with time constant τ_s. The synaptic time course is described by:

$$ds_i(t)/dt = -s_i(t)/\tau_s. \quad (4)$$

Throughout the song, each LMAN input is modeled as an independent Poisson process, with a constant mean firing rate $\lambda = 80Hz$ (5). This firing rate was based on estimates of the song system in Leonardo et al. (2004) (5). In the real system there are weak correlations between LMAN activity and song. Our model ignores these correlations and treats LMAN simply as a pure source of exploration with completely random inputs. We do not believe that introducing a more complex experimenter would change our results because the same HVC synapses would continue to be influenced by overlapping LMAN activity.

c. <u>The Motor Pools</u>

Song production is modeled by two non-spiking motor-pool output units that receive input from RA. These motor pools represent premotor nuclei controlling song features such as fundamental frequency and amplitude, and are defined by:

$$\tau_m\, dm_k(t)/dt + m_k(t) = \sum_i A_{ki} s_i^{RA}(t) + b_k, \qquad (5)$$

where each motor pool has time constant τ_m and tonic activation b_k. Each motor pool sums activity from RA weighted by a fixed set of output weights A. Half of the RA neurons project to motor pool 1 (m_1) and half to motor pool 2 (m_2). Half of m_1 RA neurons are excitatory ($A_{ki} > 0$) and half are inhibitory ($A_{ki} < 0$).

The goal of learning in the model is for the two motor pools to reproduce a target motor trajectory. To generate this trajectory, the weight matrix was assigned random values on the interval [0, 4]; this led to a particular trajectory of motor-pool activity and was used as the target motor trajectory for subsequent learning throughout our study.

2. Learning Parameters

In our model, only HVC projections to RA are plastic. These changes are determined by

$$dW_{ij}/dt = \eta R(t) e_{ij}(t), \quad (6)$$

where R(t) is the reinforcement signal at every time point t in the song motif, and η is the learning rate. η determines the size of the synaptic changes after each trial, and was empirically determined for the longer simulations and optimized to have a stable, decreasing error. The eligibility for plasticity at each synapse, at each time point, $e_{ij}(t)$, is defined by:

$$e_{ij}(t) = \int_0^t dt' \, G(t-t') \, (s_i^{LMAN}(t') - < s_i^{LMAN} >) \, s_{ij}^{HVC}(t'), \quad (7)$$

where $G(t) = t^n e^{t/\tau_e}$, n=5, and time constant $\tau_e = 5ms$. For learning to occur, coincident activity from HVC and LMAN must occur at a single RA site.

The eligibility trace is chosen to be non-zero when there are coincident LMAN and HVC activity based on two ideas. First, LMAN activity perturbs song by influencing the RA patterns of activation, and the song perturbations that improve performance are then consolidated in the HVC to RA pathway. When LMAN activity is high, and song is better than expected, this implies the additional, chance input from LMAN improved the song. In order to consolidate this improvement, the weights from HVC to RA are changed in the direction of the eligibility value: higher than average inputs from LMAN result in a positive eligibility trace and strengthens the HVC to RA synapses that were active at that moment in song. Likewise, if inputs from LMAN are low and song is better than expected, this implies that reduced input to RA from LMAN improved the song. In this scenario, the eligibility trace is negative and weakens synapses from HVC to RA that were active at that moment. Second, this type of eligibility trace implies a form of input-timing-dependent synaptic plasticity (ITDP) at the HVC-RA-LMAN nexus. Such a form of plasticity has been found in slice experiments in RA (6). The exact shape of our eligibility trace is not crucial to our results: the key aspect is that HVC cells which synapse onto the same RA cell and fire at nearby times would be similarly influenced by LMAN activity.

Calculating eligibility is computationally intensive. To speed up simulation time, we compute the convolution using Fourier transforms.

a. Learning Dynamics

The reinforcement signal is created by comparing the motor pool outputs with the target motor trajectory and is defined as:

$$R(t) = 2 * \Theta[D(t) - \bar{D}(t)] - 1, \quad (8)$$

where Θ is the Heaviside function, $D(t)$ is the time delayed activity for a trial and $\bar{D}(t)$ is the adaptive threshold calculated by averaging the past five trials of $D(t)$. Five trials were chosen such that reward was calculated relative to a recent expectation of song quality, as has been shown experimentally in Gadagkar et al. (2016) (7). The exact number of trials is not experimentally constrained and was chosen based on Fiete et al. (2007) (2). We do not believe the exact number qualitatively impacts our modeling results. $D(t)$ is defined as:

$$D(t + T_{delay}) = -([\bar{m}_1(t) - m_1(t)]^2 + [\bar{m}_2(t) - m_2(t)]^2). \quad (9)$$

Thus, when performance is better than the average of the previous five trials, the reinforcement signal is +1 and when it is worse than the average of the previous five trials, reinforcement is -1. Error shown in figures is the absolute difference between the target and actual motor-pool activity summed across both motor pools.

When the network first starts a trial, there must be enough HVC cells active to drive the rest of the network. To prevent such edge effects from entering our calculations, we confined our analyses of error to within a conservative window, defined as the middle 100 ms of the song.

B. Perturbations to HVC sequencing

In the following sections, we describe the network configurations used to perturb HVC and the implementation of the tests of robustness. To model changes in HVC firing, we define an "epoch" in the learning process by a given number of iterations of the song: N_{stop}. After each epoch a perturbation event occurs. We vary the number of perturbations from zero to fifty, and extend the simulation as needed beyond 100,000 iterations to provide a complete unperturbed final epoch of song. For each number of perturbations, we simulate 50 trials with different randomly generated initial weight matrices, by selecting the random seed.

We chose punctate perturbation events for simplicity in our simulations and based on the experimental observation by Liberti et al (2016) that more changes in HVC activity appear to happen overnight when the bird is not singing (8). However, we believe that our results would be the same if we were to allow perturbations to happen continuously over the course of singing and would likely even improve the overall performance of song since a continuous method of perturbation would not generate the punctate jumps in error that our schemes do.

1. HVC Perturbations: Pausing with Synaptic Weakening

500 HVC neurons were active on each song iteration; 200 additional HVC neurons were paused. At the end of each epoch, we perturbed HVC by randomly sampling 30 neurons from the conservative window of the "active pool" of HVC cell to be placed in this "paused pool" and sample 30 neurons from the "paused pool" to enter the active pool. While neurons are in this paused pool, their synapses undergo synaptic weakening via the following equation:

$$\frac{dW_{ij}^{paused}}{dt} = -(W_{ij}^{paused} - W_{ij}^{initial})/\tau_{LTD}, \quad (10)$$

where W_{ij}^{paused} is the current synaptic weight of the i[th] synapse of the paused j[th] HVC neuron and $W_{ij}^{initial}$ is the initial paused synaptic weight. In this way, the synaptic weights of paused neurons decay back to their initial values.

2. HVC Perturbations: Pausing

This framework utilizes the same network configurations as above without synaptic weakening. While neurons are in the paused pool, all of the associated synapses are frozen until placed back into the active pool.

3. HVC Perturbations: Time-Shifts

In these simulations there are 500 active neurons in the HVC layer. At the end of each epoch, we perturb HVC by randomly choosing 5% of the cells and shifting their burst-onset times randomly within the song (Fig. 2). The new times are chosen using the equation:

$$t_{new} = \Delta t + t_{old}, \qquad (11)$$

where Δt is drawn from a uniform distribution between $[-t_{old}, T - t_{old}]$, where T = length of the song.

C. Exploring the Impact of Perturbations on Network Robustness

To test the robustness of the network, we developed three measures. First, we quantified the ability of the network to learn the target activity under different numbers of perturbations. Next we changed the target song and investigated the speed and quality of relearning. Finally, we simulated RA neuron loss and measured the error introduced in the song.

1. Error Reduction

To quantify how well the network learned the template, we defined the measure of “error improvement” as the difference between the initial error and the average of the last 500 iterations.

2. Cell Loss in RA

We halted activity in subpopulations (1/12 of the network) of RA, and analyzed how this affected performance error. The loss of neurons was restricted so that losses were equal for both the m_1 and m_2 motor pools. We repeated this test over 500 randomly drawn subpopulations and report the mean resulting error.

3. Shifts in Song and Relearning

To shift the target song, we added a gaussian waveform, with temporal width $\sigma = 10\,ms$, centered at the midpoint of the song to the original template motor-pool activity (Fig. 2c). To calculate the speed of relearning, we measured the time to half decay of the error.

D. Origins of Robustness

1. Quantifying network change due to HVC perturbations: pairwise correlation of HVC synaptic weights

The pairwise correlation between individual HVC neurons' synaptic weights was calculated as a function of the difference in timing between the HVC neurons' burst onsets. We denote the outgoing weights for HVC neuron *p* at time *t* as $W^t{}_p \equiv W^t{}_{(:,p)}$. For all pairs of HVC projection vectors, $W^t{}_p$ and $W^{t'}{}_q$ for which the HVC neurons' burst-onset times *t* and *t'* are within $\tau \pm \Delta\tau$, we compute the average pairwise correlation at time separation τ, as:

$$C_\tau(W^t{}_p, W^{t'}{}_q) = \left\langle \frac{(W^t{}_p - \overline{W^t{}_p})(W^{t'}{}_q - \overline{W^{t'}{}_q})}{\sqrt{(W^t{}_p - \overline{W^t{}_p})^2 (W^{t'}{}_q - \overline{W^{t'}{}_q})^2}} \right\rangle_{all\ p,q:\ (t-t') \subseteq \tau \pm \Delta\tau} \quad (10)$$

We compute C_t for all timing intervals τ between 0 and 50 ms; we take $\Delta\tau$ = 0.5 ms. To track network development, these correlations were computed every 200 iterations throughout learning.

2. Effect of network change on relearning speed: generation of correlated, Gaussian-distributed random weight matrices

To test our hypothesis that increasing correlations in the synaptic projections between HVC cells that fired at nearby times slows re-learning, we generated random weight matrices such that,

$$W^t{}_p = r W_p{}^{(t+\delta t)} + (1 - r^2) * \overline{X} \qquad (11)$$

where $\overline{X}$ is a vector of independent gaussian random variables with $\mu = 5$ and $\sigma^2 = 1$, $W_p{}^{(t+\delta t)}$ are the synaptic weights from the HVC cell which fires at the smallest latency after the HVC cell that fires at time t with synaptic weights, $W_p{}^t$, and r is the correlation strength between these two HVC projection vectors. Changing r changes the pairwise correlation between different HVC neurons' synaptic projection strengths without changing the overall distribution of weights. We then used these weight matrices as initial conditions for 3,000 iterations of song learning. We measured the relative speed of learning a function of initial correlation strength and found that higher correlations in the initial weight matrix lead to slower learning speeds. See figure S4 for results.

3. Effect of network change on relearning speed: generation of random weight matrices from different weight distributions

To compare the effect of correlations within the weight matrices on re-learning speed to the effect of synaptic strengths on re-learning speed, we similarly generated two sets of random initial weight matrices drawn from two different weight distributions. We generated the first set of weights from the synaptic weight distribution of the control (0 perturbation) set of weights (SI Appendix, Fig. S2b) and the second set of weights from the synaptic weight distribution of the 50 perturbation set of weights (SI Appendix, Fig S2b). In both sets, the correlations in the matrices were zero.

We then used these weight matrices as initial conditions for 3,000 iterations of learning. We found that the distribution of initial weights had no significant impact on re-learning speed (0 perturbation distribution time to half decay = 107.5+-9.8 iterations, 50 perturbation distribution time to half decay = 127.1 +- 15.4 iterations; variation is standard error; each set contains 10 trials). This suggests that the change in weight distributions across perturbation conditions (SI Appendix, Fig. S2b) does not impact re-learning speeds.

4. Quantifying network change due to HVC perturbations: analysis of RA activity and participation within song

After all of the maintenance song iterations and HVC perturbations were complete, we quantified the resulting RA activity patterns during song. For each HVC perturbation scheme, the average activity of RA cells per song was calculated by simulating 50 song realizations of a single final weight matrix with different LMAN activity and no learning. Next, we summed across time to count the total number of spikes in a song per RA cell. We averaged across the 50 different learned realizations of the song to establish the average number of spikes per song per final weight matrix. We then repeated this for all final weight matrices (N=50). We plot the histogram of these average spike counts in figure S5a-c.

Using the previous simulations we calculated the cell participation within each time bin by counting the number of RA cells with spikes in each time bin. Time bins were chosen to be 0.5 milliseconds long. We plot the histogram of RA cell participation in figure S5d-f.

5. Effect of network change on robustness to cell loss: impact of RA sparseness on m_1 and m_2 activity

Based on the analysis in the previous section 3, we then considered what the effects of changes in RA activity would have on robustness to cell loss in RA. Because of the feedforward nature of the song system, synaptic activity from RA neurons sum to drive changes in m_1 and m_2 (see SI Appendix eq. 5). HVC perturbations lead to sparser RA activity during song: fewer RA neurons fire at any single time point in song and the average firing rate of RA neurons is lower (SI Appendix, Fig. S5). As a result of sparser RA activity, when a single RA neuron is removed from network, the change in activity in the motor pool layer is lower in proportion to the firing rate of the RA neuron (see SI Appendix eq. 5). The efficiency of sparse RA activity means that any one RA neuron's contribution to the motor pool output is less critical.

6. Linear Analysis of correlated LMAN input

We analytically study the effects of correlated LMAN inputs on the buildup of correlations in the W matrix by considering a linear, discrete-time version of our learning system. In this reduced model, we assume that time is discrete and that at each timestep in song, j, a single, binary HVC input is active. RA activity is defined by the sum of active synaptic weights onto each RA neuron plus an input from LMAN which is drawn from a Gaussian distribution, $\xi_{hj} = \mathcal{N}\sim(0, \sigma_L)$, and is independent to each cell. We define the correlation of ξ_{hj} across time steps in song as: $corr(\xi_{h,j}, \xi_{h,j+r}) \equiv c_L(r)$ where r is the number of discrete time steps separating the LMAN inputs. We assume that the RA network projects to a single, time varying output variable, m, which is defined as the sum of the RA activity at each time step weighted by a static projection weight vector, A_i, whose elements are drawn independently from a Gaussian distribution, $A_i = \mathcal{N}\sim(0, \sigma_a)$ for a single network realization. 'm' at time step j is thus,

$$m^j = \sum_{h=1}^{N_{RA}} A_h(W_{hj} + \xi_{hj}).$$

We quantify network performance by comparing the network output, m^j, to a target output, $\bar{m}^j$: $R_j^{\xi} = \left(\bar{m}^j - m^j\right)^2 = \left(\bar{m}^j - \left[\sum_{i=1}^{N_{RA}} A_i\left(W_{ij} + \xi_{ij}\right)\right]\right)^2$. We define a reinforcement signal as the difference between this network performance and a noiseless version of the network, which we define as: $R_j^0 = \left(\bar{m}^j - m^j\right)^2 = \left(\bar{m}^j - \left[\sum_{i=1}^{N_{RA}} A_i\left(W_{ij}\right)\right]\right)^2$ (2). The reward function is therefore:

$$R_j = R_j^0 - R_j^{\xi}.$$

When the noise input from LMAN improves the performance of the network relative to no noise input, R_j is positive, and when the noise input from LMAN results in worse performance, R_j is negative. At the Nth iteration of learning, the weight from the jth HVC neuron to the hth RA neuron is given by:

$$w_{hj}^N = w_{hj}^0 + \sum_{n=1}^{N} \Delta w_{hj}^n.$$

w_{hj}^0 is the initial, random weight value and Δw_{hj}^n is the change in weight w_{hj} on the *n*th song iteration. We define the learning rule for the change in weights at each song iteration, *n*, as:

$$\Delta w_{hj}^n = \eta R_j^n \xi_{hj}^n,$$

where R_j^n is R_j evaluated on the *n*th song iteration, and η is the learning rate that determines how much each weight changes at each song iteration (2). This learning rule is a discrete adaptation of the original learning rule.

We wish to determine whether positive correlations in the noise inputs from LMAN lead to positive correlations in weights of neighboring HVC inputs. To do this, we calculate the covariance of neighboring weight changes within a single song iteration with respect to all LMAN inputs: $\langle \Delta w_{hj}^n, \Delta w_{h,j+r}^n \rangle_{\xi_{aj}^n, \xi_{aj+r}^n;\, a=1:N_{RA}} = E\left[\Delta w_{hj}^n\, \Delta w_{h,j+r}^n\right] - E\left[\Delta w_{hj}^n\right] E\left[\Delta w_{h,j+r}^n\right]$.

Expanding the terms in R_j, we find

$$R_j^n = 2\bar{m}_j \sum_{i=1}^{N_{RA}} \xi_{ij}^n A_i - 2\sum_{i=1}^{N_{RA}} \sum_{k=1}^{N_{RA}} w_{ij}^n \xi_{kj}^n A_i A_k - \sum_{i=1}^{N_{RA}} \sum_{k=1}^{N_{RA}} \xi_{ij}^n \xi_{kj}^n A_i A_k.$$

So,

$$\Delta w_{hj}^n = 2\eta \xi_{hj}^n \bar{m}_j \sum_{i=1}^{N_{RA}} \xi_{ij}^n A_i - 2\eta \xi_{hj}^n \sum_{i=1}^{N_{RA}} \sum_{k=1}^{N_{RA}} w_{ij}^n \xi_{kj}^n A_i A_k - \eta \xi_{hj}^n \sum_{i=1}^{N_{RA}} \sum_{k=1}^{N_{RA}} \xi_{ij}^n \xi_{kj}^n A_i A_k.$$

The covariance $\langle \Delta w_{hj}^n, \Delta w_{h,j+r}^n \rangle$ can be divided into nine sums of covariances. In computing the terms in the covariance, we assume that $w_{hj}^n \geq 0$ for all w_{hj}^n. This assumption comes from the parameters of the bird song system: HVC to RA projections are excitatory. We make use of Isserlis' theorem to compute the high order terms of the multivariate gaussians in the covariance expression. The sign of portions of the covariance depends on the specific realizations of A_i's. The A_i variables are arbitrarily chosen output weights from RA to the motor pool that are independently drawn from a Gaussian distribution, $A_i = \mathcal{N}\sim(0, \sigma_a)$, at the beginning of a learning trial and are fixed throughout. Thus, we take the expectation over A_i's over different realizations of this network.

After evaluating each term in the covariance expression as described above, we get this final expression:

$$\langle \Delta w_{hj}^n, \Delta w_{h,j+r}^n \rangle = 4\eta^2 (\sigma_L^2 c_L(r))^2 \sum_{k=1,\neq h}^{N_{RA}} \left(3\sigma_a^2 (w_{k,j+r}^n w_{kj}^n) + \sum_{p=1,\neq k}^{N_{RA}} \sigma_a^4 (w_{p,j+1}^n w_{pj}^n) \right)$$
$$+ 8\eta^2 c_L^2(r) \left(3\sigma_a^2 w_{h,j+r}^n w_{hj}^n + \sigma_a^4 \sum_{p=1,\neq h}^{N_{RA}} w_{p,j+r}^n w_{pj}^n \right) + 4\eta^2 (\sigma_L^2 c_L(r))^2 m_j m_{j+r} (N-1)\sigma_a^2$$

$$+ 8\eta^2 m_j m_{j+r} \sigma_a^2 c_L^2(r)$$
$$+ \eta^2 \sigma_a^4 \Big[4(N-1)(\sigma_L^6 c_L(r) + 2c_L^3(r)\sigma_L^2) + \left(6\sigma_L^4 c_L(r)(N-1) \right)$$
$$+ 4(N-1)(N-2)c_L^3(r)\sigma_L^6 + 2(N-1)(N-2)c_L(r)\sigma_L^6$$
$$+ 3(N-1)(\sigma_L^6 c_L(r) + 2c_L^3(r)\sigma_L^2) + 9(2\sigma_L^6 c_L^3(r) + 3\sigma_L^6 c_L(r)) \Big].$$

This expression shows that all terms of this covariance are, on average, non-negative under some assumptions about $m_j \; and \; m_{j+r}$: (1) either $E[m_j m_{j+r}] \geq 0$ or (2) the values of all m_j are the same sign. It is unlikely that $E[m_j m_{j+r}] < 0$ for small r, given that our time step between j and j+1 is small, 0.5 ms, and, in general, there would be correlations in neighboring portions of a motor sequence. Note, that all $w_{ij} \geq 0$, so while we do not calculate the explicit values of the sums, these terms are always positive. Correlations in LMAN input add to the magnitude of the covariance of changes in w.

If $E[m_j m_{j+r}] \geq 0$ but $corr(\xi_{h,j}, \xi_{h,j+r}) = 0$, then $\langle \Delta w_{hj}^n, \Delta w_{h,j+r}^n \rangle = 0$. This shows that correlations in LMAN inputs are necessary for driving correlations in the weight changes in this simple model.

Lastly, this simple model shows why either temporarily silencing HVC cells or randomly changing their timing within the sequence would slow the growth of correlations in the synaptic

weights: cells would be exposed to less correlated LMAN activity because there would be iterations where $corr(\xi_{h,j}, \xi_{h,j+r}) = 0$.

Parameters

Conductance model	Description	Parameter name	Value
	Membrane capacitance	Cm	$1\ \mu F/cm^2$
	Leak equilibrium potential	V_L	-60 mV
	HVC leak conductance	g_L	0.3 mS/cm^2
	RA leak conductance	g_L	0.44 mS/cm^2
	Action potential threshold	V_θ	-50 mV
	Reset potential	V_{reset}	-55 mV
Connectivity	Weight Matrix	W	
	Paused Steady State Weights	$W^{initial}$	
	Paused Pool Weights	W_{Paused}	
	RA Neuron Count	N_{RA}	48
	HVC Active Neuron Count	N_{HVC}	500
	HVC Paused Neuron Count	$N_{HVC\ Paused}$	200
	LMAN Neuron Count	N_{LMAN}	48
Synaptic parameters	Synaptic Time Constant	τ_s	5 ms
Motor Pool	Motor Pool Time Constant	τ_m	5 ms
	Tonic Activation 1	b_1	60
	Tonic Activation 2	b_2	40
	RA Positive Output Weights 1	A_{ij}	$440/N_{RA}$

	RA Negative Output Weights 1	A_{ij}	$-440/N_{RA}$
	RA Positive Output Weights 2	A_{ij}	$660/N_{RA}$
	RA Negative Output Weights 2	A_{ij}	$-660/N_{RA}$
Learning	Learning Rate	η	$5 * 10^{-5}$
	Eligibility Time Constant	τ_e	5 ms
	Iterations in a Epoch	N_{stop}	50,000-2,000
	Number of Epochs	N_{Epoch}	1-50
	LTD Time COnstant	τ_{LTD}	.001
	Number of neurons place in paused pool	N_{change}	30 Each

Supplementary Bibliography

1. Stark, L. L. and D. J. Perkel (1999). "Two-stage, input-specific synaptic maturation in a nucleus essential for vocal production in the zebra finch." J Neurosci **19**(20): 9107-9116.
2. Fiete IR, Fee MS, Seung HS (2007) Model of birdsong learning based on gradient estimation by dynamic perturbation of neural conductances. J Neurophysiol 98(4):2038–2057.
3. Hahnloser RH, Kozhevnikov AA, & Fee MS (2002) An ultra-sparse code underlies the generation of neural sequences in a songbird. Nature 419(6902):65-70.
4. Spiro JE, Dalva MB, Mooney R (1999) Long-range inhibition within the zebra finch song nucleus RA can coordinate the firing of multiple projection neurons. J Neurophysiol 81(6):3007–20.
5. Leonardo A (2004) Experimental test of the birdsong error-correction model. Proceedings of the National Academy of Sciences of the United States of America 101(48):16935-16940.

6. Mehaffey WH & Doupe AJ (2015) Naturalistic stimulation drives opposing heterosynaptic plasticity at two inputs to songbird cortex. Nature Neuroscience 18(9):1272-1280.
7. Gadagkar V, et al.(2016) Dopamine neurons encode performance error in singing birds. Science 354(6317):1278-1282.
8. Liberti WA, 3rd, et al.(2016) Unstable Neurons Underlie a Stable Learned Behavior. Nature Neuroscience 19(12):1665-1671.